PHOTOCLINOMETRY FROM SPACECRAFT IMAGES

CONTRIBUTIONS TO ASTROGEOLOGY

GEOLOGICAL SURVEY PROFESSIONAL PAPER 599-B

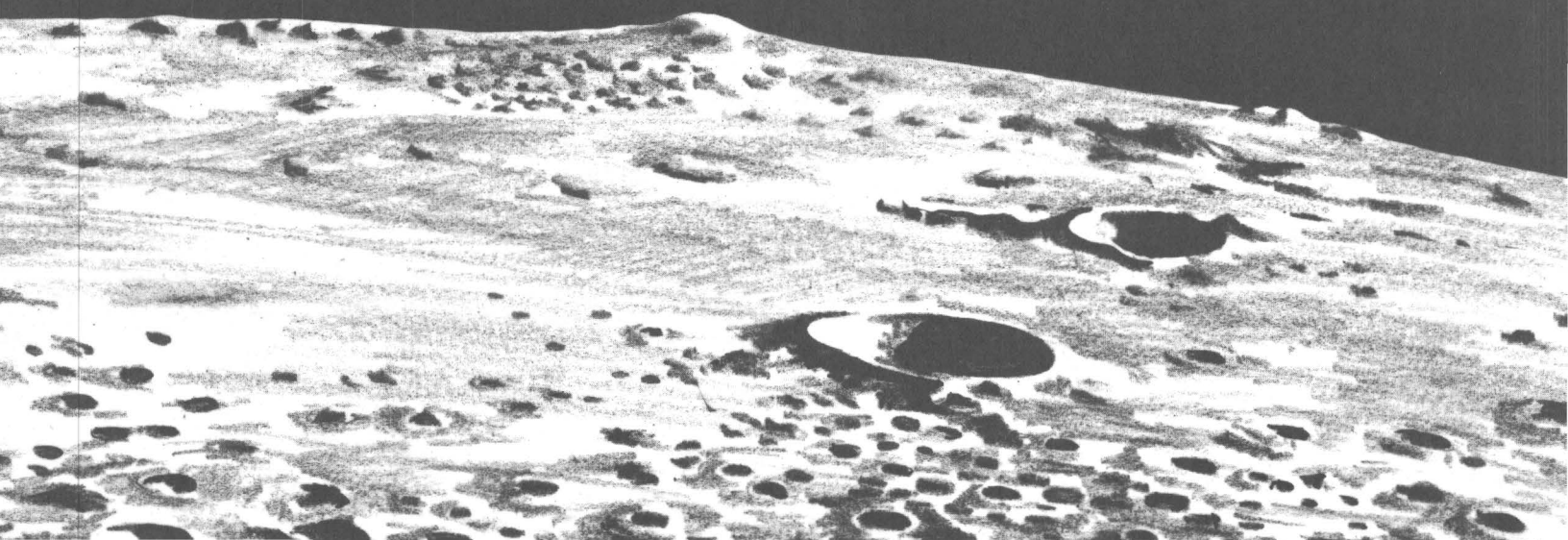

Photoclinometry From Spacecraft Images

By KENNETH WATSON

CONTRIBUTIONS TO ASTROGEOLOGY

GEOLOGICAL SURVEY PROFESSIONAL PAPER 599-B

UNITED STATES GOVERNMENT PRINTING OFFICE, WASHINGTON : 1968

UNITED STATES DEPARTMENT OF THE INTERIOR

STEWART L. UDALL, *Secretary*

GEOLOGICAL SURVEY

William T. Pecora, *Director*

For sale by the Superintendent of Documents, U.S. Government Printing Office
Washington, D.C. 20402 - Price 20 cents (paper cover)

CONTENTS

ILLUSTRATIONS

CONTRIBUTIONS TO ASTROGEOLOGY

PHOTOCLINOMETRY FROM SPACECRAFT IMAGES

By KENNETH WATSON

ABSTRACT

Photographic and photoelectric photometry of the moon from the earth has been interpreted to imply that the brightness at any point, corrected for the normal albedo, is dependent only on the brightness longitude and the phase angle. Extrapolation of these interpretations to spacecraft observations has resulted in a technique designed to compute topographic profiles along the intersection of phase planes with the ground surface. Although relative profiles can be constructed from spacecraft images, the independence of brightness to slope components in directions other than phase plane intersections implies that these profiles cannot be connected together in a unique manner solely from photometric considerations of a single photograph. The application of photoclinometry combined with limited photogrammetry to provide high-resolution topographic maps for Surveyor and Orbiter will be restricted in the former case to the science flights which will use high-resolution stereographic cameras to study the terrain in the immediate vicinity of the spacecraft, and in the latter case by the topographic control provided by the medium-resolution stereographic photographs.

INTRODUCTION

The term "photoclinometry" denotes a technique used to extract slope information from an image brightness distribution. The word is derived from the Greek noun "phos" (light) and the Latin verb "clinare" (to bend). When this technique is applied to the lunar surface, the reflection characteristics of the moon or the photometric function must first be considered, since the technique is primarily dependent on the precision with which the lunar photometric function is known.

More than 300 years ago Galileo first observed that at full moon every point on the lunar surface reaches maximum brightness. If the moon were a smooth, diffusely reflecting sphere, however, the limbs would show darkening. Over the last 300 years these preliminary visual observations by Galileo have been extended by detailed photographic and photoelectric photometry studies to extract information on the surface roughness and behavior of the moon under reflected sunlight (Barabashov, 1922; Markov, 1924; Markov and Barabashov, 1926; Fessenkov and others, 1928; Sharonov, 1936; Sytinskaya, 1948; Fedoretz, 1952; van Diggelen, 1959; Wildey and Pohn, 1964; Gehrels and others, 1964.)

Öpik (1924) concluded that the photometric functional form is nearly the same for all types of lunar geologic rock types, and Minnaert (1961) demonstrated that this functional form has a remarkable property: the brightness at any point, corrected for the normal albedo, is dependent only on the brightness longitude and the phase angle. Wildey and Pohn tested the brightness dependence on the elevation angles of the earth and sun for a short range of phase angles and concluded that a dependence on only the phase and the brightness longitude angles is reasonably well approximated.

To provide some extrapolation of terrestrial observations to spacecraft images it will be assumed that the photometric function is independent of scale. Photogrammetric information from the images will be required in order to examine this assumption more critically.

GEOMETRY OF THE PHOTOMETRIC FUNCTION

Figure 1 represents a block of lunar surface material. It shows the path of a ray from the sun to a point on the lunar surface (the incident ray) and the ray reflected back to the observer or the spacecraft (the emergent ray). The phase angle is defined as the angle between the incident ray and the emergent ray and is measured in a plane containing both rays—the phase plane. No matter how the block is tilted about the observed surface point, the phase angle remains constant. Brightness longitude is defined as an angle measured in the phase plane between the emergent ray to the observer (fig. 1) and a line perpendicular to the intersection of the ground with this plane.

If the block is rotated about the line of intersection with the phase plane, the brightness longitude remains constant. If the block is tilted along an axis at right angles to this line of intersection, the brightness longitude changes. The brightness at any point is, therefore,

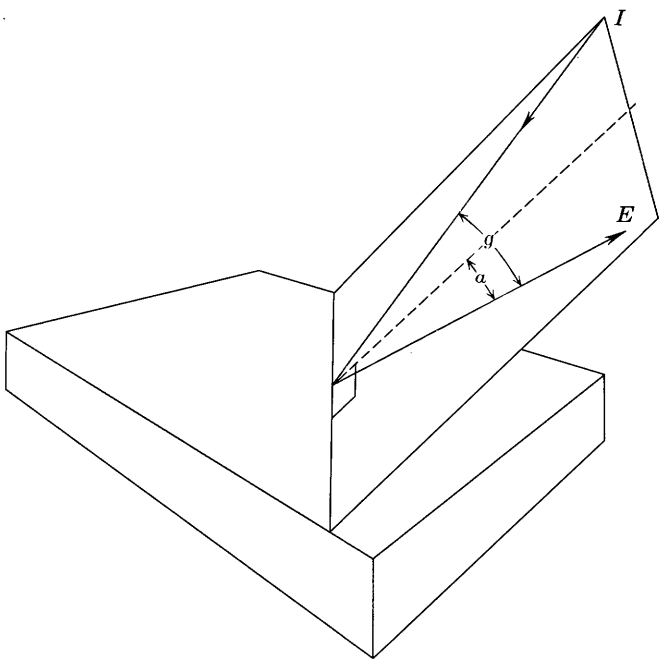

FIGURE 1.—Relationship between the brightness longitude (α), the phase angle (g), and the incident (I) and emergent (E) (or observing) rays.

dependent only upon the slope component in the phase plane, the normal albedo, and the phase angle.

In the case of earth-based lunar observations, the ray from the sun to the moon (incident ray) and the ray from the earth to the moon (emergent ray) remain essentially in a plane paralleling the ecliptic. Because the ecliptic intersects the moon nearly along latitude lines, the brightness of the moon, corrected for albedo variations, is independent of latitude. Topographic slope components from terrestrial photographs were first measured by van Diggelen (1951) in an investigation of mare ridges and were later applied by Dale (1962) to the general topography of the maria. Wilhelms (1963) extended the technique to a variety of different lunar terrains, and McCauley (1965) expanded this work to produce a detailed quantitative terrain map of the lunar equatorial belt at a scale of 1:2,000,000.

Two photometric functions, based on different assumptions, have been derived from earth-based observations. The first is that of Hapke, which was derived by parametric fitting from theoretical considerations of a scattering model of the lunar surface (Hapke, 1963; revised model, 1966). The second, based entirely on lunar photographic data, was derived completely empirically by Herriman, Washburn, and Willingham (1963) and by Willingham (revised model, 1964).

In figure 2, which shows the four functions mentioned above, brightness is plotted as a function of brightness longitude and phase angle. It is important to note that one of the major limitations in constructing a photometric function from terrestrial observations is that a particular lunar feature cannot be observed for a wide variety of earth-angle observations. This is primarily because the libration in longitude of the moon is only $\pm 8°$, so that data can be obtained only on a single feature over a rather narrow range of brightness longitudes. In addition, most compiled lunar photometric observations are subject to the photographic-technique limitations described by Pohn (1965).

EXTRACTION OF TOPOGRAPHIC INFORMATION FOR A GEOLOGICALLY HOMOGENEOUS AREA

The two-dimensional image brightness distribution of a geologically homogeneous area of the lunar surface (that is, an area of constant normal albedo and photometric function) is dependent only on the phase angle (g) and the brightness longitude (α). The intersection of a particular phase plane with an arbitrary rough surface (fig. 3) illustrates the dependence of the brightness longitude on slope components rather than on true slopes.

Because the sun's rays to the lunar surface are nearly parallel and because every phase plane must contain the lens nodal point, it follows that all phase planes of the set characterized by a single camera station intersect along a common line, which is the particular sun's ray which passes through the lens nodal point. This line intersects the ground surface at a point which is the shadow of the lens nodal point, and since the incident and emergent rays to this point coincide, it also represents the point of zero phase angle. The images of the phase plane set are a family of straight lines radiating out from the image of the lens nodal shadow point. Derivation of the image grid coordinates of this point from the known spacecraft configuration is described in the next section. This formulation was based on the tabulated data for the Ranger spacecraft and is compatible with the spacecraft geometry format of the Unmanned Lunar Orbiter.

Figure 4 illustrates the relationship between the change in phase angle (Δg), and the brightness longitude (α) and the range change (ΔR) for two adjacent rays which lie in the same phase plane. Range (R) is the distance between the lens nodal point and the intercept of the optic axis with the ground. The geometry has been enlarged in figure 5 to show more clearly the derivation of the equation for the range along a particular phase plane profile. Since the phase angle at each point on the profile can be computed directly (that is, the phase angle at any image point is the angle subtended at the lens nodal point by the image point and the image of the lens nodal shadow point) and since the brightness longitude can be computed from the bright-

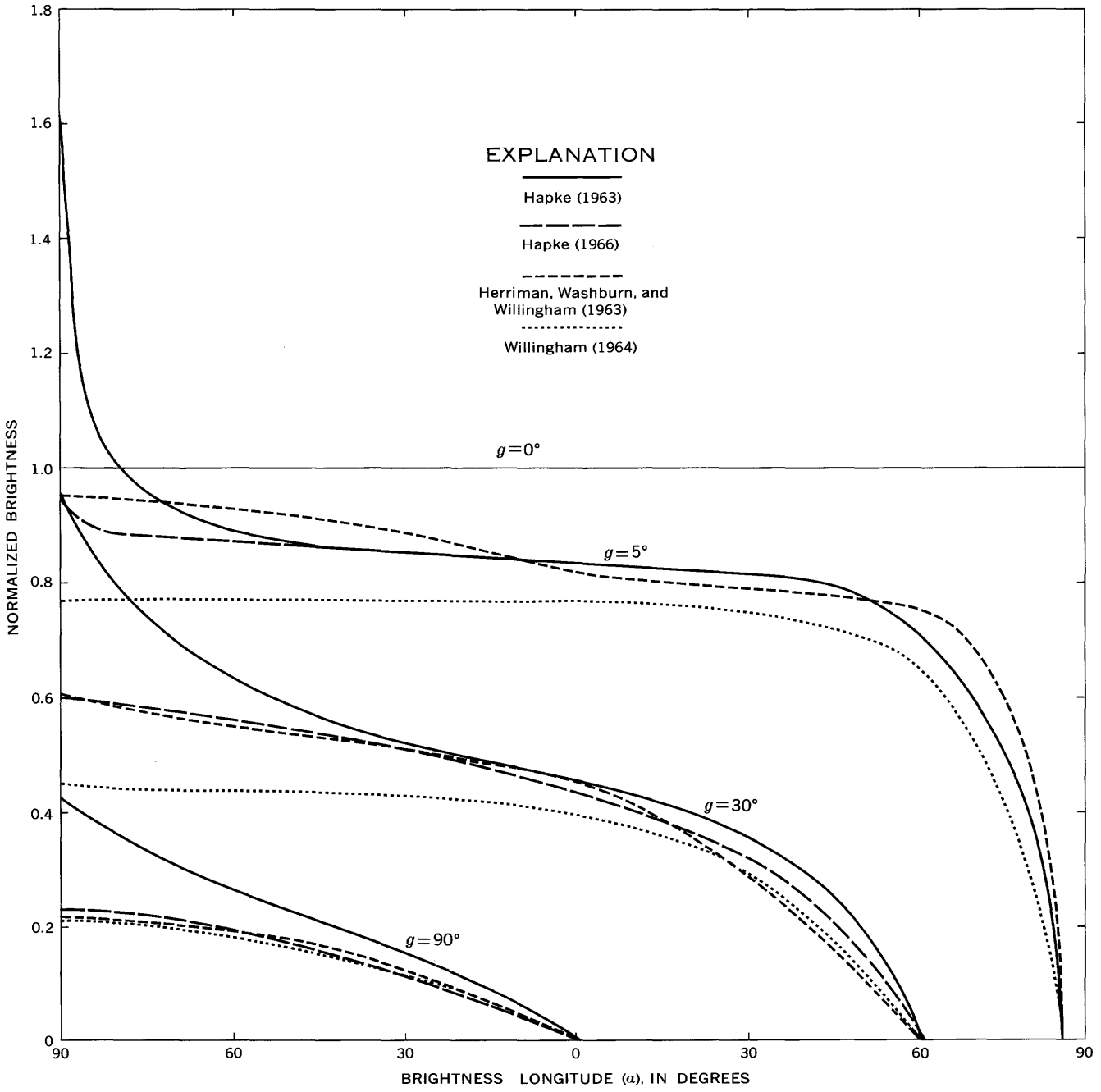

FIGURE 2.—Lunar photometric functions; brightness (normalized to unity at $g=0°$) is plotted as a function of brightness longitude (α) and phase angle (g).

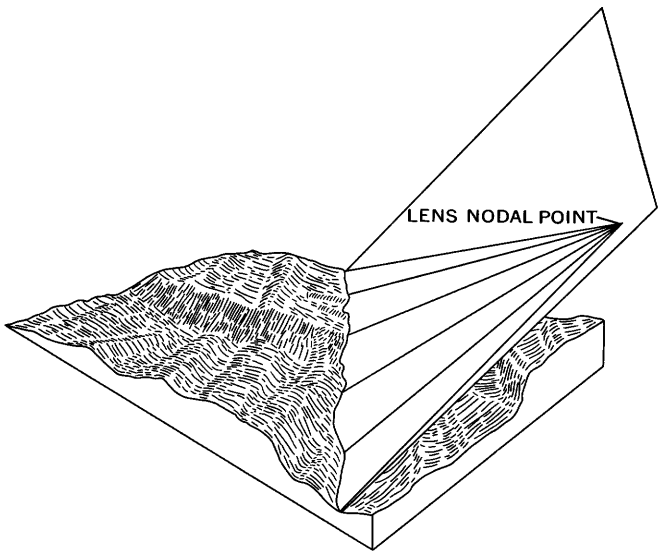

FIGURE 3.—Intersection of a phase plane with a rough surface. Dependence of brightness on slope component and deviation of phase plane trace from colinearity are both illustrated.

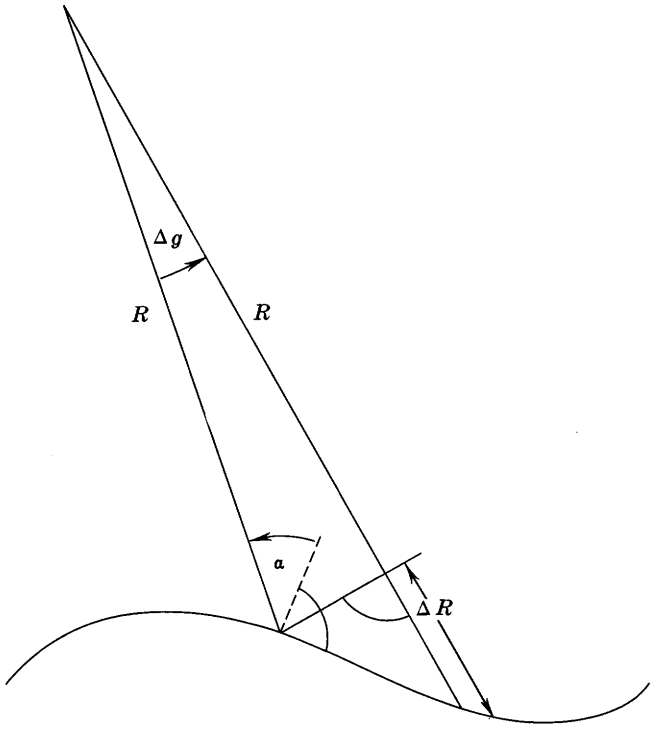

FIGURE 4.—Phase plane geometry for two adjacent rays from the lens nodal point to the ground profile. R=range; Δg= small phase angle difference between adjacent rays (positive counterclockwise); α=brightness longitude (positive counterclockwise); ΔR=range change.

ness at the image point and an assumed photometric function, then the range to each individual profile point can be computed except for the arbitrary integration constant, R'. There will, of course, be a different integration constant for each phase plane profile; thus

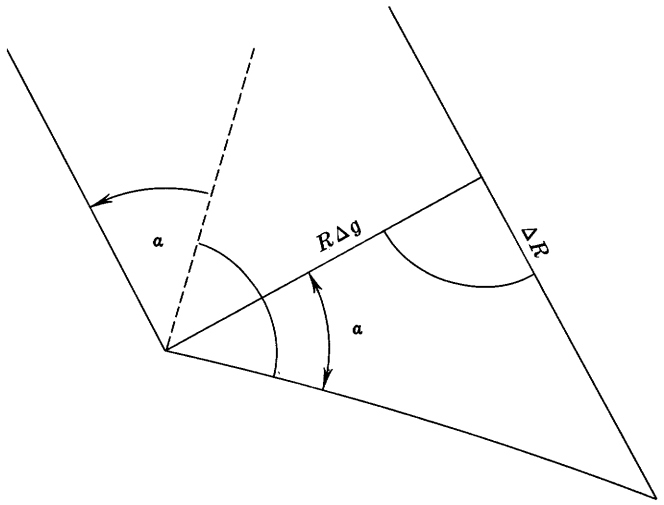

FIGURE 5.—Enlarged geometry of figure 4 and the mathematical derivation:

$$\tan \alpha = \Delta R / R \Delta g;$$

therefore $\Delta R = R \Delta g \tan \alpha.$

As $\Delta g \rightarrow dg;$

$$\Delta R \rightarrow dR;$$

therefore $dR/R = \tan \alpha \, dg,$

and $$\int_{R'}^{R} dR/R = \int_{g'}^{g} \tan \alpha \, dg$$

$$R = R' \exp\left(\int_{g'}^{g} \tan \alpha \, dg\right).$$

the individual profiles cannot be linked together without additional assumptions or qualitative judgement. Previous maps produced by this method were constructed either by selecting a featureless area within the photograph as a datum plane or by simplifying statistical assumptions concerning the average slope of adjacent profiles. In the final analysis, however, some type of independent control, such as that derived by photogrammetry, is required in order to arrive at an unambiguous topographic solution. However, statistical analysis of the slope components can be used to classify different surface materials according to relative roughness without the necessity of linking the profiles together.

A simplified derivation of the topographic solution is presented in a later section (p. B6) to illustrate the computation of the Cartesian coordinates of individual points from the range information. It is important to recognize, however, that in a nonhomogeneous area variations in both normal albedo and brightness longitude contribute to changes in a single image brightness distribution. Thus their individual contributions to the brightness at any point cannot be separated mathematically.

DERIVATION OF THE IMAGE PLANE COORDINATES OF THE LENS NODAL SHADOW POINT

The following treatment represents a derivation of the equations necessary to compute the image plane coordinates of the lens nodal shadow point from the selenographic coordinates of the optic axis intercept with the ground and the subspacecraft point, the lens focal length, the grid deviation from north, and the range-altitude distances. The image of the family of phase planes is a set of lines radiating from the image of the lens nodal shadow point; hence, the required brightness profile directions are completely specified by the coordinates of this point.

A Cartesian coordinate system is used with origin at the center of the moon, x axis through the mean libration center, z axis through the north pole, and y axis from the right-hand rule. All distances are normalized by dividing them by the mean lunar radius; thus, the rectangular coordinates of a point on the lunar surface at latitude λ, longitude β, are:

$$x=\cos\lambda\cos\beta,$$

$$y=\cos\lambda\sin\beta,$$

and

$$z=\sin\lambda.$$

Prime symbols designate points in the image plane, and the following subscripts indicate particular points:

$*$=subsolar point,

I=zero phase angle point,

s=lens nodal point,

o=intercept of optic axis with ground,

ss=subspacecraft point,

and

n=point north of o.

The sun's ray through the lens nodal point is parallel to the line joining the subsolar point to the center of the moon and contains the image of the zero phase angle point and the lens nodal point.

$$\frac{x_I'-x_s}{x_*}=\frac{y_I'-y_s}{y_*}=\frac{z_I'-z_s}{z_*}. \tag{1}$$

Now the camera optic axis contains the lens nodal point, the center reticle point, and the intercept of the optic axis with the ground.

$$\frac{x_o'-x_s}{x_s-x_o}=\frac{y_o'-y_s}{y_s-y_o}=\frac{z_o'-z_s}{z_s-z_o}. \tag{2}$$

The focal length distance, f, is equal to the distance between the lens nodal point and the center reticle.

$$f=[(x_o'-x_s)^2+(y_o'-y_s)^2+(z_o'-z_s)^2]^{1/2}. \tag{3}$$

The range, R_o, is equal to the distance between the lens nodal point and the intercept of the optic axis with the ground.

$$R_o=[(x_s-x_o)^2+(y_s-y_o)^2+(z_s-z_o)^2]^{1/2}. \tag{4}$$

Combining equations 2, 3, and 4 yields:

$$x_o'=x_s+\frac{f}{R_o}(x_s-x_o),$$

$$y_o'=y_s+\frac{f}{R_o}(y_s-y_o),$$

$$z_o'=z_s+\frac{f}{R_o}(z_s-z_o). \tag{5}$$

Since the camera optic axis is perpendicular to the image plane which contains the image of the lens nodal shadow point and the center reticle, then:

$$(x_s-x_o)(x_I'-x_o')+(y_s-y_o)(y_I'-y_o')+(z_s-z_o)(z_I'-z_o')=0. \tag{6}$$

Combining equations 1, 3, 4, and 6 yields:

$$x_I'=x_s+\frac{fR_ox_*}{\Delta_*},$$

$$y_I'=y_s+\frac{fR_oy_*}{\Delta_*},$$

$$z_I'=z_s+\frac{fR_oz_*}{\Delta_*}, \tag{7}$$

where

$$\Delta_*\equiv x_*(x_s-x_o)+y_*(y_s-y_o)+z_*(z_s-z_o).$$

The angular deviation between grid north and true north is defined as the intersection angle in the image plane between the grid north line and the longitude line, both of which contain the center reticle point. Define an arbitrary point in object space (subscript n) which lies on the longitude line through the intercept of the optic axis with the ground. The image coordinates of this point can be derived in a similar fashion to the image coordinates of the center reticle (eq 5) and the image coordinates of the lens nodal shadow point (eq 7).

$$x_n'=x_s+\frac{fR_o(x_s-x_n)}{\Delta_n},$$

$$y_n'=y_s+\frac{fR_o(y_s-y_n)}{\Delta_n},$$

$$z_n'=z_s+\frac{fR_o(z_s-z_n)}{\Delta_n}, \tag{8}$$

where

$$\Delta_n \equiv (x_s-x_o)(x_s-x_n)+(y_s-y_o)(y_s-y_n)+(z_s-z_o)(z_s-z_n).$$

Now introduce a two-dimensional Cartesian coordinate system $(\bar{x}, \bar{y})$ whose origin is at the center reticle point and whose $\bar{y}$ axis points toward grid north. The image plane coordinates of the lens nodal shadow point $(\bar{x}_I, \bar{y}_I)$ are given by

$$\bar{x}_I=\rho_I \sin(\theta_I+\alpha),$$

$$\bar{y}_I=\rho_I \cos(\theta_I+\alpha),$$

where ρ_I is the distance from the center reticle, θ_I the angle between the true north image line and the line from the center reticle to the nodal shadow point image, and α the deviation of grid north from true north.

If $\vec{A}$ and $\vec{B}$ are image plane vectors from the center reticle to true north and to the nodal shadow point image, respectively, then:

$$\sin\theta_I=(\vec{A}\times\vec{B})\cdot\hat{C}/AB, \tag{9}$$

$$\cos\theta_I=\vec{A}\cdot\vec{B}/AB, \tag{10}$$

$$\rho_I=B, \tag{11}$$

where $\hat{C}$ is a unit vector away from the ground, along the optic axis.

$$\vec{B}=\vec{B}(x_I'-x_o', y_I'-y_o', z_I'-z_o'), \tag{12}$$

$$\vec{A}=\vec{A}(x_n'-x_o', y_n'-y_o', z_n'-z_o'), \tag{13}$$

and

$$\hat{C}=\hat{C}[(x_o'-x_s)/f, (y_o'-y_s)/f, (z_o'-z_s)/f]. \tag{14}$$

Define the following quantities:

$$\Delta_{*n}\equiv x_*(x_s-x_n)+y_*(y_s-y_n)+z_*(z_s-z_n),$$

$$\Delta_{sn}\equiv (x_s-x_n)^2+(y_s-y_n)^2+(z_s-z_n)^2,$$

and

$$\Delta_{*sn}\equiv x_*[(y_s-y_o)(z_s-z_n)-(y_s-y_n)(z_s-z_o)]$$
$$+y_*[(x_s-x_n)(z_s-z_o)-(x_s-x_o)(z_s-z_n)]$$
$$+z_*[(x_s-x_o)(y_s-y_n)-(x_s-x_n)(y_s-y_o)].$$

The final results are summarized below:

$$\rho_I=f[(R_o/\Delta_*)^2-1]^{1/2},$$

$$\cos\theta_I=f[(R_o^2\Delta_{*n}/\Delta_*\Delta_n)-1]/\rho_I[(R_o^2\Delta_{sn}/\Delta_n^2)-1]^{1/2},$$

$$\sin\theta_I=+[R_o(f)\Delta_{*sn}/\Delta_n\Delta_*]/\rho_I[(R_o^2\Delta_{sn}/\Delta_n^2)-1]^{1/2}.$$

To complete the calculations an expression for the north point (x_n, y_n, z_n) must be derived. Let

$$x_n=\cos(\lambda_o+\delta)\cos\beta_o,$$

$$y_n=\cos(\lambda_o+\delta)\sin\beta_o,$$

$$z_n=\sin(\lambda_o+\delta),$$

$$\lim_{\delta\to o}\frac{x_o-x_n}{z_o-z_n}=-\tan\lambda_o\cos\beta_o,$$

and

$$\lim_{\delta\to o}\frac{y_o-y_n}{z_o-z_n}=-\tan\lambda_o\sin\beta_o.$$

Since (x_n, y_n, z_n) is an arbitrary point on a line, the choice of the value of z_n is not restricted. For simplicity, z_n can be chosen equal to unity, thus

$$x_n=x_o-\tan\lambda_o\cos\beta_o(1-z_o),$$

$$y_n=y_o-\tan\lambda_o\sin\beta_o(1-z_o),$$

$$z_n=1.$$

To facilitate computation, the coordinates are re-expressed in terms of the spacecraft geometry format.

$x_*=\cos\lambda_*\cos\beta_*$,
$y_*=\cos\lambda_*\sin\beta_*$, and
$z_*=\sin\lambda_*$.

$x_o=\cos\lambda_o\cos\beta_o$
$y_o=\cos\lambda_o\sin\beta_o$, and
$z_o=\sin\lambda_o$.

$x_s=(1+A)\cos\lambda_s\cos\beta_s$,
$y_s=(1+A)\cos\lambda_s\sin\beta_s$, and
$z_s=(1+A)\sin\lambda_s$.

$x_{ss}=\cos\lambda_s\cos\beta_s$,
$y_{ss}=\cos\lambda_s\sin\beta_s$, and
$z_{ss}=\sin\lambda_s$.

$x_n=\cos\lambda_o\cos\beta_o-\tan\lambda_o\cos\beta_o(1-\sin\lambda_o)$,
$y_n=\cos\lambda_o\sin\beta_o-\tan\lambda_o\sin\beta_o(1-\sin\lambda_o)$, and
$z_n=1$.

DERIVATION OF RELATIVE OBJECT SPACE COORDINATES

A simplified scheme is derived to compute the relative object space coordinates of an image point whose associated phase angle (g) and brightness longitude (a) are known. Let T be the transformation matrix between the image grid coordinate system (z axis pointing along the camera optic axis) and the object space coordinate system (origin at the intersection of the

optic axis with the ground, z axis vertical). The transformation is chosen so that the y axes in the two coordinate systems are an image-object pair.

A point, P, has coordinates (x, y, z) in the image grid system and $(\bar{x}, \bar{y}, \bar{z})$ in the object space system, where

$$\begin{pmatrix}\bar{x}\\ \bar{y}\\ \bar{z}\end{pmatrix}=(t_{ij})\begin{pmatrix}x\\ y\\ z-R_o\end{pmatrix}$$

and the elements, t_{ij}, of T which satisfy the constraints and the orthogonality of the transformation (Morse and Feshbach, 1953) are:

$$t_{11}=(1-t_{13}^2)^{1/2},$$

$$t_{12}=0,$$

$$t_{21}=-t_{13}t_{23}/(1-t_{13}^2)^{1/2},$$

$$t_{22}=-\cos\Phi/(1-t_{13}^2)^{1/2},$$

$$t_{31}=t_{13}\cos\Phi/(1-t_{13}^2)^{1/2},$$

and

$$t_{33}=-\cos\Phi,$$

where

$$\cos\Phi=A/R_o,$$

and where

A=spacecraft altitude and
R_o=spacecraft range along the optic axis.

The elements t_{13} and t_{23} are computed from the spacecraft geometry format as follows. Introduce the unit vectors:

- $\hat{\gamma}$ is along the optic axis pointing towards the lens nodal point.
- $\hat{s}$ is the local ground normal.
- $\hat{n}$ is in the ground plane and points north from the optic axis intercept with the ground.
- $\hat{n}'$ is the image of $\hat{n}$ (that is, lying in the image plane).
- $\hat{y}$ is the image plane, passing through the center reticle and pointing toward grid north.
- $\hat{x}$ is in the image plane, passing through the center reticle and pointing toward grid east.

The grid deviation angle as defined previously is α; hence

$$\hat{y}\cdot\hat{n}'=\cos\alpha, \tag{15}$$

$$\hat{y}\times\hat{n}'=\sin\alpha\hat{\gamma}, \tag{16}$$

$$\hat{x}\cdot\hat{n}'=\sin\alpha, \tag{17}$$

$$\hat{x}\times\hat{n}'=-\cos\alpha\hat{\gamma}. \tag{18}$$

Also since the unit vector $\hat{n}$ and its image $\hat{n}'$ are coplanar with $\hat{\gamma}$, then if we define an angle ω as subtended between $\hat{\gamma}$ and $\hat{n}$ (fig. 6),

$$\hat{n}-\hat{\gamma}=\cos\omega. \tag{19}$$

But the unit vector $\hat{n}'$ lies in the image plane and hence is perpendicular to the unit vector $\hat{\gamma}$ which lies along the optic axis. Therefore

$$\hat{n}'\times\hat{\gamma}=-(\hat{n}\times\hat{\gamma})/\sin\omega, \tag{20}$$

$$\hat{n}\cdot\hat{n}'=-\sin\omega, \tag{21}$$

and

$$\hat{n}\cdot\hat{\gamma}=\cos\omega. \tag{22}$$

The matrix elements t_{13} and t_{23} are the cosines of the angles between the x and y image plane axes and the local ground normal, respectively; therefore

$$t_{23}=\hat{y}\cdot\hat{s} \tag{23}$$

and

$$t_{13}=\hat{x}\cdot\hat{s}. \tag{24}$$

From the vector analysis identity for a triple product

$$\hat{n}\times(\hat{n}'\times\hat{\gamma})=\hat{n}'(\hat{n}\cdot\hat{\gamma})-\hat{\gamma}(\hat{n}\cdot\hat{n}'). \tag{25}$$

Substitution of the results of equations 22, 21, and 20 in 24 yields

$$\hat{n}\times(\hat{n}\times\hat{\gamma})=-\sin\omega(\hat{n}'\cos\omega+\hat{\gamma}\sin\omega). \tag{26}$$

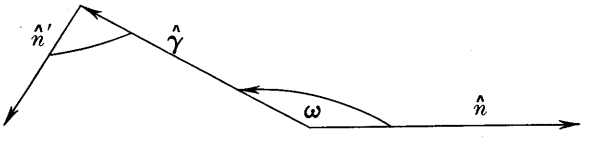

FIGURE 6.—North-pointing vector and its image.

Applying the triple product identity to the left-hand side of equation 26

$$\hat{n}\times(\hat{n}\times\hat{\gamma})=\hat{n}(\hat{n}\cdot\hat{\gamma})-\hat{\gamma}(\hat{n}\cdot\hat{n}). \tag{27}$$

Equating equations 26 and 27 and introducing the results of equation 22 into the right-hand side of 27 gives

$$\hat{\gamma}-\hat{n}\cos\omega=\sin\omega(\hat{n}'\cos\omega+\hat{\gamma}\sin\omega),$$

or, solving for $\hat{n}'$,

$$\hat{n}'=(\cos\omega\hat{\gamma}-\hat{n})/\sin\omega. \tag{28}$$

From the triple product identity we write

$$\hat{n}'\times(\hat{y}\times\hat{n}')=\hat{y}(\hat{n}\cdot\hat{n}')-\hat{n}'(\hat{n}'\cdot\hat{y}); \tag{29}$$

therefore

$$\hat{y}=\hat{n}'\times(\hat{y}\times\hat{n}')+\hat{n}'(\hat{n}'\cdot\hat{y}) \tag{30}$$

and in an identical fashion

$$\hat{x}=\hat{n}'\times(\hat{x}\times\hat{n}')+\hat{n}'(\hat{n}'\cdot\hat{x}). \tag{31}$$

Substitution of equations 16, 15, and 20 in 30 and 18, 17, and 20 in 31 results in two equations:

$$\hat{x}=[\cos\alpha(\hat{n}\times\hat{\gamma})-\sin\alpha(\cos\omega\hat{\gamma}-\hat{n})]/\sin\omega \tag{32}$$

and

$$\hat{y}=[-\sin\alpha(\hat{n}\times\hat{\gamma})+\cos\alpha(\cos\omega\hat{\gamma}-\hat{n})]/\sin\omega. \tag{33}$$

Since Φ as defined previously is the angle between $\hat{\gamma}$ and $\hat{s}$, then

$$\hat{\gamma}\cdot\hat{s}=\cos\Phi. \tag{34}$$

Substitute equations 32, 33, and 34 in 23 and 24 and define ψ as

$$\psi\equiv(\hat{n}\times\hat{\gamma})\cdot\hat{s}. \tag{35}$$

Therefore

$$t_{13}=(\psi\cos\alpha+\sin\alpha\cos\Phi\cos\omega)/\sin\omega \tag{36}$$

and

$$t_{23}=(-\psi\sin\alpha+\cos\alpha\cos\Phi\cos\omega)/\sin\omega \tag{37}$$

where ψ is defined in equation 35 and $\cos\omega$, in equation 22. Since $0<\omega<\pi$, then $\sin\omega=+(1-\cos^2\omega)^{1/2}$. To compute ψ and $\cos\omega$, the unit vectors $\hat{n}$, $\hat{\lambda}$, and $\hat{s}$ are expressed in terms of their components:

$$\hat{n}=\hat{n}(-\sin\lambda_o\cos\beta_o,\ -\sin\lambda_o\sin\beta_o,\ \cos\lambda_o) \tag{38}$$

$$\hat{s}=\hat{s}(\cos\lambda_o\cos\beta_o,\ \cos\lambda_o\sin\beta_o,\ \sin\lambda_o) \tag{39}$$

$$\hat{\gamma}=\hat{\gamma}\left[\frac{(1+A)\cos\lambda_s\cos\beta_s-\cos\lambda_o\cos\beta_o}{R_o},\right.$$

$$\frac{(1+A)\cos\lambda_s\sin\beta_s-\cos\lambda_o\sin\beta_o}{R_o},$$

$$\left.\frac{(1+A)\sin\lambda_s-\sin\lambda_o}{R_o}\right]. \tag{40}$$

Substitution of equations 38, 39, and 40 in 35 yields

$$\psi=(1+A)\cos\lambda_s\sin(\beta_s-\beta_o)/R_o \tag{41}$$

and substitution of equations 38 and 40 in 22 yields

$$\cos\omega=(1+A)(-\sin\lambda_o\cos\lambda_s\cos(\beta_o-\beta_s)+\cos\lambda_o\sin\lambda_s)/R_o. \tag{42}$$

Equations 36 and 37 in conjunction with equations 41 and 42 define the two transformation elements t_{13} and t_{23} in terms of the spacecraft geometry format. The final results are summarized below:

$$t_{13}=(\psi\cos\alpha+\sin\alpha\cos\Phi\cos\omega)/\sin\omega$$

and

$$t_{23}=(-\psi\sin\alpha+\cos\alpha\cos\Phi\cos\omega)/\sin\omega,$$

where

$$\psi=-(1+A)\cos\lambda_s\sin(\beta_s-\beta_o)/R_o,$$

$$\cos\omega=(1+A)(-\sin\lambda_o\cos\lambda_s\cos(\beta_o-\beta_s)+\cos\lambda_o\sin\lambda_s)/R_o,$$

and

$$\sin\omega=+(1-\cos^2\omega)^{1/2}.$$

Thus all the elements of the matrix T are specified for the transformation from image grid to object space coordinates.

Let $\vec{R}$ be the range vector (in image coordinate system) from the lens nodal point to the ground and $\vec{r}$ be the ray vector (in image coordinate system) from the associated image point to the lens nodal point. Since $\vec{R}$ and $\vec{r}$ are colinear,

$$\frac{\vec{R}}{R}=\frac{\vec{r}}{r}. \tag{43}$$

Recall the equation from figure 5:

$$R=R'\exp\left(\int_{g'}^{g}\tan\alpha dg\right). \tag{44}$$

Now equation 44 is in the correct form provided that the sign correction on dg (that is, positive counterclockwise) is observed. To ensure this, equation 44 can be rewritten as

$$R=R'\exp\left[\delta gg'\left(\frac{g-g'}{|g-g'|}\right)\int_{g'}^{g}\tan\alpha dg\right] \tag{45}$$

where $\delta gg'=+1$ if the rays fan out counterclockwise in the phase plane from the starting ray and $\delta gg'=-1$ if they fan out clockwise.

If (x_{ss}, y_{ss}), (x', y'), and (x, y) are the respective image plane points for the subspacecraft image point, the

starting point of the profile, and the ending point of the profile, then the convention on dg requires that

$$\delta gg' = \frac{(x'-x_{ss})(y-y_{ss})-(x-x_{ss})(y'-y_{ss})}{|(x'-x_{ss})(y-y_{ss})-(x-x_{ss})(y'-y_{ss})|}$$

and is derived from the scalar triple product identity.

Let $\vec{R}$ be the range vector in object space coordinates; then since T is the transform matrix between image and object space coordinates,

$$\vec{\bar{R}} = T\vec{R}. \tag{46}$$

Combining equations 43, 46, and 45 yields

$$\vec{\bar{R}} = T\vec{r}\left(\frac{R'}{r}\right)\exp\left[\delta gg'\left(\frac{g-g'}{|g-g'|}\right)\int_{g'}^{g}\tan a\,dg\right]. \tag{47}$$

Now the slope component angle (S) between two adjacent traces can be computed directly from equation 47. Since S involves the ratio of lengths which are proportional to R', then S is independent of R'. Thus slope components can be computed directly:

$$\sin S = \frac{\cos a}{R}\frac{d\bar{z}}{dg} \tag{48}$$

$$= \frac{-\cos a}{r}\left[(t_{13}/\partial g/\partial x)+(t_{23}/\partial g/\partial y) + \left(\delta gg'\tan a - \frac{1}{r}\frac{dr}{dg}\right)(t_{13}x+t_{23}y-t_{33}f)\right]. \tag{49}$$

FUTURE SPACEFLIGHT APPLICATIONS

Unmanned Lunar Orbiter provides medium-resolution photographs (10 meters) with sufficient overlap so that conventional photogrammetric techniques can be employed to extract topographic data. Nested in the center of these photographs are high-resolution (1 meter) pictures with no overlap between each other. The application of photoclinometry to these latter images requires that information from the medium-resolution images be used both to tie the topographic profiles together and to determine the effects of albedo variations to be expected in the high-resolution mode. The method will be limited by the overall quality of the photogrammetry (50-meter contours may be the best attainable), and this may be insufficient to provide adequate control. The optimum topographic control which is required for Apollo site certification may impose the requirements that each area photographed in the high-resolution mode be measured both at or near zero phase angle to determine the detailed normal albedo variations and at low sun angle lighting to provide the maximum contrast in brightness versus slope. Additional photography at lighting conditions such that the lens nodal shadow point is at significantly different orientation with respect to the area observed at high resolution could be used to tie individual profiles together in a rigorous way even though the geometrical attitude of the spacecraft with respect to the viewed area and the narrowness of the camera field of view would probably make these overlapping high-resolution images unsuitable for accurate photogrammetry.

The Surveyor science flights (two TV cameras) will provide a photogrammetric solution out to a distance of 25 meters from the spacecraft. Photoclinometry can provide supplementary profile information extending beyond the region of photogrammetric control, and these profiles can be tied together within the 25-meter radius circle. The Surveyor engineering flights (one TV camera) will be subject to the same limitations as the Unmanned Lunar Orbiter flights, and their ability to convey quantitative topographic information on the small-scale structures of the lunar surface will be limited. An improvement of this data is provided by the ability of the single camera to observe the brightness of a single surface element at different sun lighting conditions; thus, it may be possible to extract normal albedo variations and to compute intersecting phase plane profiles which can be joined together.

SUMMARY

The two-dimensional image brightness distribution obtained from lunar spacecraft observations contains both geologic and topographic information. The reflection characteristics of the lunar surface enable the application of simplified techniques to provide both topographic control and statistical slope analysis of different geologic rock units. However, careful geologic interpretation of the data in these images is necessary to extract meaningful topographic data.

REFERENCES

Barabashov, N. P., 1922, Bestimmung der Erdalbedo und des Reflexionsgesetzes fur die Oberfläche der Mondmeere—Theorie der Rillen: Astron. Nachr., v. 217, p. 445–452.

Dale, E. D., 1962, The application of the van Diggelen method of slope analysis to lunar domes and wrinkle ridges: Manchester, England, Univ. Manchester, thesis, 46 p.

Diggelen, J. van, 1951, A photometric investigation of the slopes and heights of the ranges of hills in the maria of the moon: Netherlands Astron. Inst. Bull., v. 11, p. 283–289.

——— 1959, Photometric properties of lunar crater floors: Utrecht Observatory Recherches Astron., v. 14, no. 2, 114 p.

Fedoretz, V. A., 1952, Photographic photometry of the lunar surface [in Russian]: Kharkov Univ. Astron. Observatory Trudy, v. 2, p. 49–172; *also*, Kharkov Univ. Uchenye Zapiski, v. 42, p. 49–172.

Fessenkov, B., Staude, N., and Parenago, P., 1928, Photometry of the moon: Moscow Astrophys. Inst. Trudy, v. 4, no. 1, p. 1–19.

Gehrels, T., Coffeen, T., and Owings, D., 1964, Wavelength dependence of polarization, III, the lunar surface: Astron. Jour., v. 69, p. 826–852.

Hapke, B., 1963, A theoretical photometric function for the lunar surface: Jour. Geophys. Research, v. 68, p. 4571–4586.

——— 1966, An improved theoretical lunar photometric function: Astron. Jour., v. 71, no. 5, p. 333–339.

Herriman, A., Washburn, H., and Willingham, D., 1963, Ranger preflight science analysis and the lunar photometric model: California Inst. Technology Jet Propulsion Lab. Tech. Rept. 32–384.

Markov, A., 1924, Les particularities dans la reflexion de la lumiere par la surface de la lune: Astron. Nachr., v. 221, p. 65–78.

Markov, A., Barabashov, N. P., 1926, On the reflection of light from the lunar surface [in English with Russian abs.]: Astron. Zhur., v. 3., p. 55–66.

McCauley, J. F., 1965, Terrain analysis of the lunar equatorial belt: U.S. Geol. Survey open-file report, 44 p.

Minnaert, M., 1961, Photometry of the moon, *in* Kuiper, G. P., and Middlehurst, B. M., eds., Planets and satellites, Volume 3 *of* The solar system: Chicago, Univ. Chicago Press, p. 213–245.

Morse, P. M., and Feshbach, H., 1953, Methods of theoretical physics: New York, McGraw-Hill Book Co., p. 23.

Öpik, E., 1924, Photometric measures on the moon, and the earth-shine: Tartu Univ. Astron. Observatory Pub., v. 26, no. 1, p. 1–68.

Pohn, H. A., 1965, A systematic program of photoelectric and photographic photometry of the moon, *in* Lunar and planetary investigations, Part A *of* Astrogeologic studies annual progress report, July 1963–July 1964: U.S. Geol. Survey open-file rept., p. 79–83.

Sharonov, V. V., 1936, On the determination of the absolute reflectivity of the moon and of planetary surfaces [in English with Russian abs.]: Leningrad Astron. Observatory Trudy, v. 6, p. 26–33; *also*, Leningrad Univ. Uchenye Zapiski, no. 1, p. 26–33.

Sytinskaya, N. N., 1948, Absolutnaya fotometria protyazhennykh nebesnykh obyektov: Leningrad, Zhdanov Univ. Press.

Wildey, R. L., and Pohn, H. A., 1964, Detailed photoelectric photometry of the moon: Astron. Jour., v. 69, no. 8, p. 619–634.

Wilhelms, D. E., 1963, A photometric technique for measurement of lunar slopes, *in* Studies for space flight program, Part D *of* Astrogeologic studies annual progress report, August 1962–July 1963: U.S. Geol. Survey open-file rept., p. 1–12.

Willingham, D., 1964, The lunar reflectivity model for Ranger Block III analysis: California Inst. Technology Jet Propulsion Lab. Tech. Rept. 32–664.

U.S. GOVERNMENT PRINTING OFFICE : 1968—O-273-050